Available online at www.sciencedirect.com
ScienceDirect
Surface & Coatings Technology 202 (2008) 3029–3042
SURFACE & COATINGS TECHNOLOGY
www.elsevier.com/locate/surfcoat

Growth of carbon nanotubes and microfibers over stainless steel mesh by cracking of methane

L.Z. Gao [a,*], L. Kiwi-Minsker [b], A. Renken [b]

[a] School of Mechanical Engineering M050, The University of Western Australia, 35 Stirling Highway, Crawley WA 6009, Australia
[b] École Polytechnique Fédérale de Lausanne, EPFL-LGRC, CH-1015 Lausane, Switzerland

Received 16 July 2007; accepted in revised form 3 November 2007
Available online 12 November 2007

Abstract

The La_2NiO_4 film was synthesized on the 304 stainless steel (SS) mesh. The hydrogen reduction of La_2NiO_4 generated homogeneous nano-catalyst particles (probably Ni/La_2O_3) over which methane was cracked, producing carbon nanotubes/microfibers and hydrogen. The carbon nanotubes/microfibers were strongly bonded to the SS mesh. It was observed that the methane conversion always reached its maximum at the cracking temperature of 750 °C regardless of its concentration varying from 5% to 100%. The cracking of 5% methane diluted in nitrogen generated multiwalled carbon nanotubes while the cracking of 10–100% methane resulted in the formation of carbon solid microfibers together with globular carbon particles. Higher concentration of methane created thicker carbon fibers and a 30% concentration of methane resulted in the highest deposits of carbon on the mesh. After a compressed air blow and ultrasonic treatment, the carbon deposits were still strongly adhered to the mesh. As a result of the carbon tubes/fibers coverage, the specific surface area of the SS mesh was enhanced significantly from 0.03 m^2/g to 21–45 m^2/g. XRD, HRTEM and Raman studies confirmed that the carbon products were of graphitic structure. Such advanced mesh material would have great application potential in industrial catalysis and other areas.

Keywords: Stainless steel; La_2NiO_4 film; Methane cracking; Carbon fibers; Specific surface area

1. Introduction

Compared with a conventional bed of catalyst pellets, catalysts made of metal wire mesh have many advantages including lower pressure drop, higher thermal conductivity, mechanical strength, electromagnetic shielding, uniform fluid flow, less stagnation zones and hot-spots [1,2]. Wire mesh catalysts of precious metals (such as Pt, Ru, Ag) have long been used in the production of nitric acid from ammonia and formaldehyde from methanol [3]. These mesh catalysts, however, have low specific surface areas and are highly expensive as they consist of homogeneous bulk metal wires. There have been attempts to utilize wire meshes made of cheap iron or stainless steel as support of active catalyst component. A number of cheap wire mesh reactors have been used in the field of pyrolysis [4,5], the coal/char gasification and combustion [6] and catalytic oxidation of 1,2-dichlorobenzene [7]. The surface area of metal mesh is too low, high surface area is one of the most important factors for catalyst support. To improve the surface area of metal mesh is a necessary but difficult task to achieve.

Carbon nanofibers (CNFs) and nanotubes (CNTs) are important materials which can be applied in many areas such as electrodes, adsorbents, lubricants, hydrogen storage, catalyst support etc. Metal foils covered with CNFs or CNTs could provide a gas impermeable layer, of high value for cryogenic or liquid fuel (e.g. LNG) storage applications. CNFs or CNTs are usually synthesized on the powder catalysts and need further separation and purification. In many cases, the application requires re-dispersion and reattachment of CNTs or CNFs to a support structure. One approach is to use polymer binder [8]. However, such method occludes much of the carbon nanofiber or nanotube' surface area. On the other hand, the polymer bound carbon nano materials are unstable at high temperatures. If the CNFs or CNTs can directly grow on the metal substrate, the reattachment of CNTs will become unnecessary. It is particularly important to have the CNFs or CNTs anchored

* Corresponding author.
E-mail address: lizhen@mech.uwa.edu.au (L.Z. Gao).

0257-8972/$ - see front matter © 2007 Elsevier B.V. All rights reserved.
doi:10.1016/j.surfcoat.2007.11.006

firmly on the supporting material. Weakly attachment would lead to loss of the CNFs or CNTs during practical application along with a loss of the desired property.

If CNFs or CNTs can be directly grown on stainless steel mesh with good adhesion then, the specific surface area of mesh could be enhanced dramatically and the further practical application of CNFs and CNTs would become a practical viable alternative. The diamond-like carbon films was deposited on stainless steel substrates using plasma-assisted chemical vapor deposition (PACVD) from either methane, acetylene, or 1,3-butadiene precursors with argon or hydrogen as a dilute [9,10]. Amorphous carbon was created on the stainless steel to lower the friction [11]. CNTs were synthesized on the stainless steel tube for gas separation. Prior to the growth of CNTs, the Co-Mo catalyst needed to coat on the mesh [12].

Methane catalytically creaking to produce hydrogen and CNFs or CNTs is of significant importance because of its low cost, easy handling and scaling up [13]. It is also an alternative for methane fuel cell as this process will not produce either CO_2 or CO. The present reaction routes in the methane fuel cell are methane steam reforming ($CH_4+H_2O\rightarrow H_2+CO$) and partial oxidation ($CH_4+O_2\rightarrow CO+H_2$). However, these two ways both produce CO which will deactivate the fuel cell electrode and need subsequent WGS reaction ($CO+H_2O\rightarrow CO_2+H_2$). The CNFs and CNTs are also in turn promising fuel cell electrode substrates. If we employ the mesh supported CNFs or CNTs as fuel cell electrodes, the design of fuel cell device will be more flexible.

CNFs or CNTs synthesis *via* CVD is typically a two-step process. The first step involves the coating of the substrate with the catalyst, or the metal impregnation of a catalyst support. Subsequent heat treatment leads to the formation of nano-particles. Catalyst coatings have been deposited by spin coating [14], dip coating [15], sputtering [16] and sol–gel techniques [17]. The catalysts are usually possessed of the element of Fe, Co or Ni [18–23]. Whereas few papers about the growth of CNTs and CNFs on metal mesh using methane as a carbon source are encountered in the literature. Randall et al synthesized CNTs over the stainless steel mesh by use of either C_2H_2/C_6H_6 or CO/C_6H_6 as carbon sources [24]. Riccardis et al made CNTs over the Ni/carbon fibres catalysts by using acetone as the carbon source [25]. Tzeng et al grew carbon nanofibers over the carbon fiber fabrics by using the methane cracking method [26].

Coating the inorganic catalysts over metal wire is usually carried out by the conventional wash-coating method, in which a finite thickness of a supporting layer is formed on the surface of the wire by repeatedly dipping the wire into a slurry that contains particles of the inorganic materials, followed by drying and calcinating [27]. The catalyst layer that is formed by the wash-coating method sometimes does not adhere well to the wire surface. The coatings may flake away under the influence of mechanical stresses and vibration. Several other techniques have been investigated to obtain strongly adherent coatings with a large surface area such as plasma spray deposition [28,29], plasma electrolytic oxidation (PEO) [30] and the electrophoretic deposition (EPD) method [31]. M.P. Vorob'eva et al coated active alumina over a wire mesh by using PEO method [32].

In the present study, we synthesized La_2NiO_4 catalyst on the stainless steel mesh on which carbon microfibers and nanotubes were grown by the cracking of CH_4.

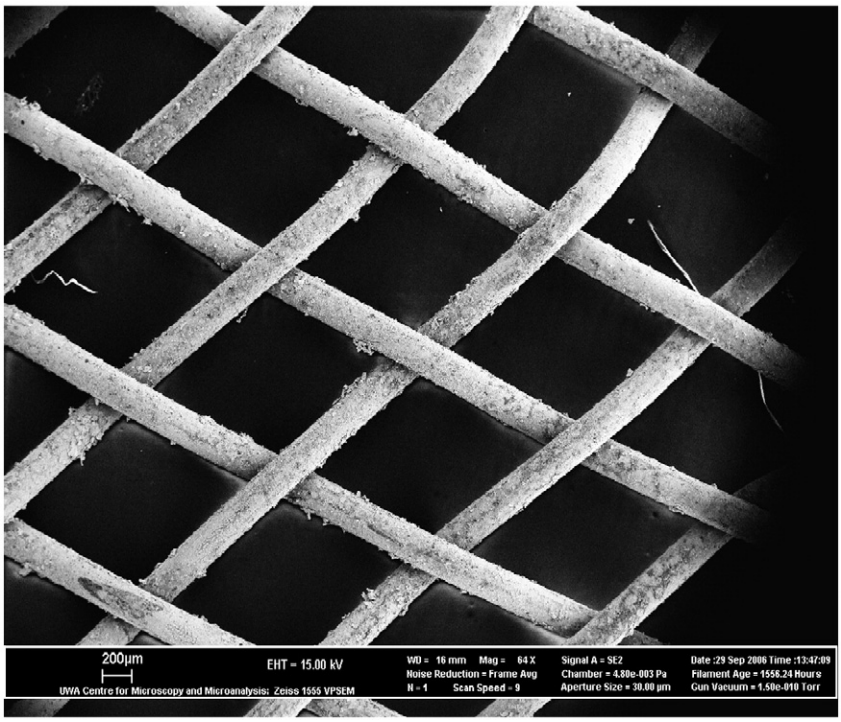

Fig. 1. SEM image of the SS mesh after blasting with by fine sand flow.

2. Experimental

2.1. Catalyst coating on the stainless steel mesh

The 304 SS mesh was used as the catalyst support. The surface of fresh mesh wire was so smooth that it was difficult to load the catalyst. Prior to catalyst loading, the mesh was blasted with fine grits in order to improve its surface roughness. The sand blasted mesh was then dipped into a boiling diluted nitric acid (30%) solution for 5 min to create a nitrate film (such as nickel nitrate or chromium nitrate) over the mesh surface which was more compatible and reactive with the nitrate catalyst precursor. The mesh was subsequently immersed into the catalyst precursor solution. The catalyst precursor solution was prepared by dissolving lanthanide nitrate and nickel nitrate into a citric acid water solution (20 g citric acid in 500 ml distilled

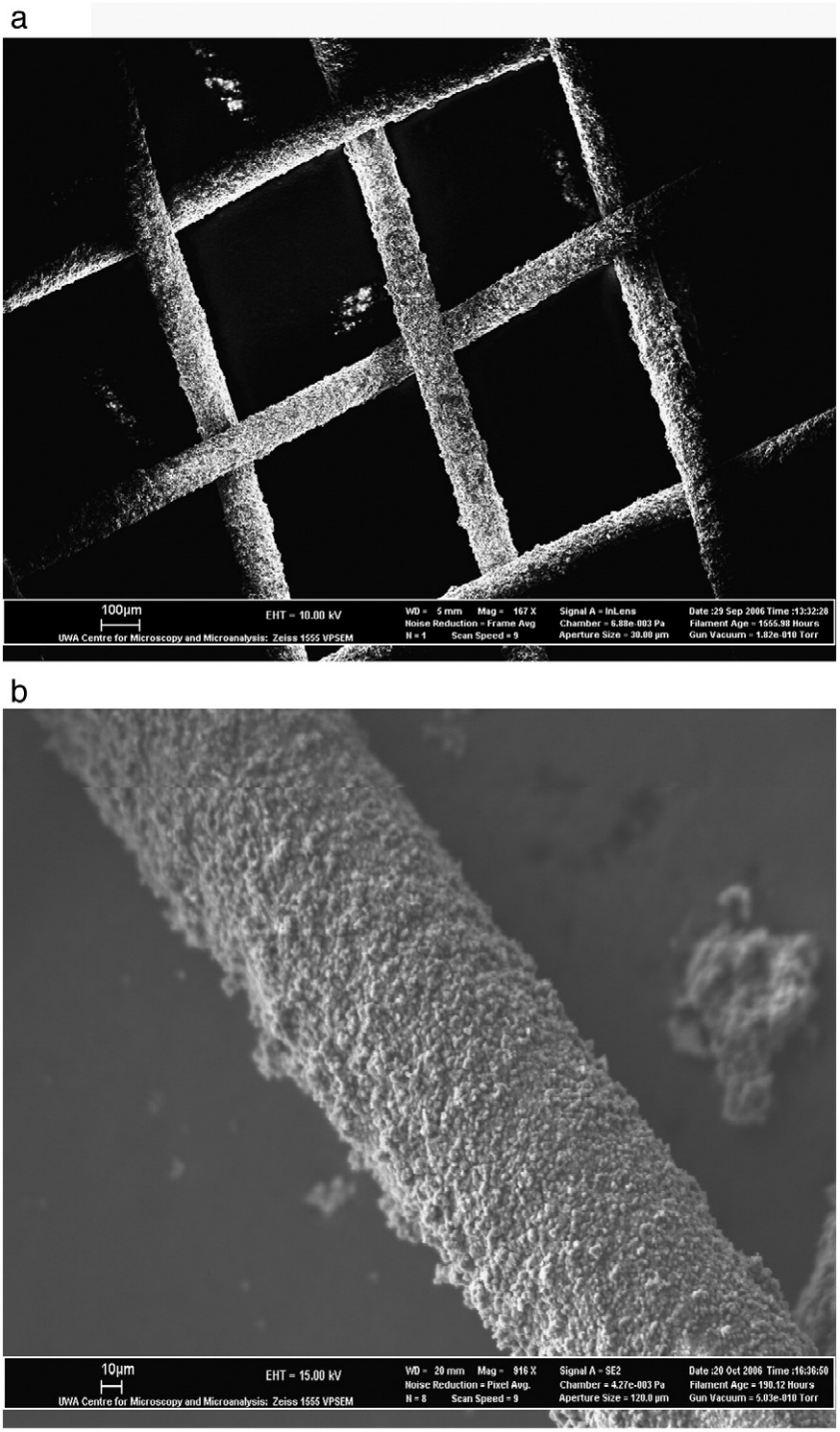

Fig. 2. SEM images of SS mesh coated with La_2NiO_4 after being heated at 800 °C in N_2.

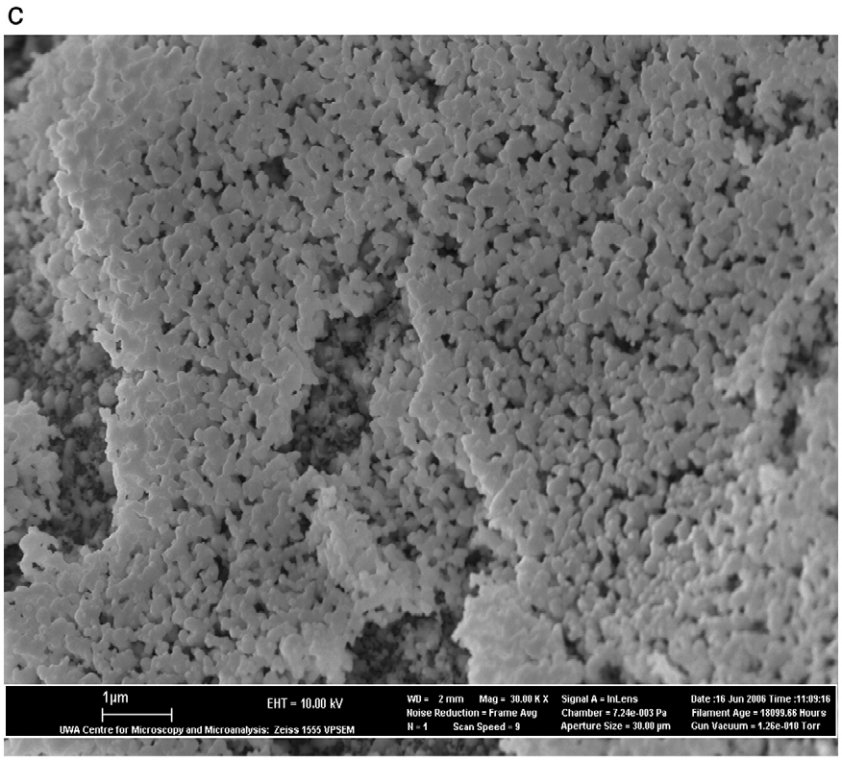

Fig. 2 (*continued*).

water) according to the stoichiometric ratio of La/Ni=2 (La $(NO_3)_3 \cdot 6H_2O$, 0.866 g; $Ni(NO_3)_2 \cdot 6H_2O$, 0.291 g. 500 ml H_2O). The solution was first heated to 80 °C with constant stirring. To keep the concentration unchanged, a condenser tube was connected to the flask. After about 20 h, the condenser tube was disconnected and the temperature was maintained at 80 °C. About 5 h later, the solution turned into a homogeneous viscous syrup. At this moment the mesh surrounded by catalyst precursor syrup was pulled out and dried at 100 °C for 1 h and calcinated in a N_2 flow at 800 °C for 5 h. In order to remove

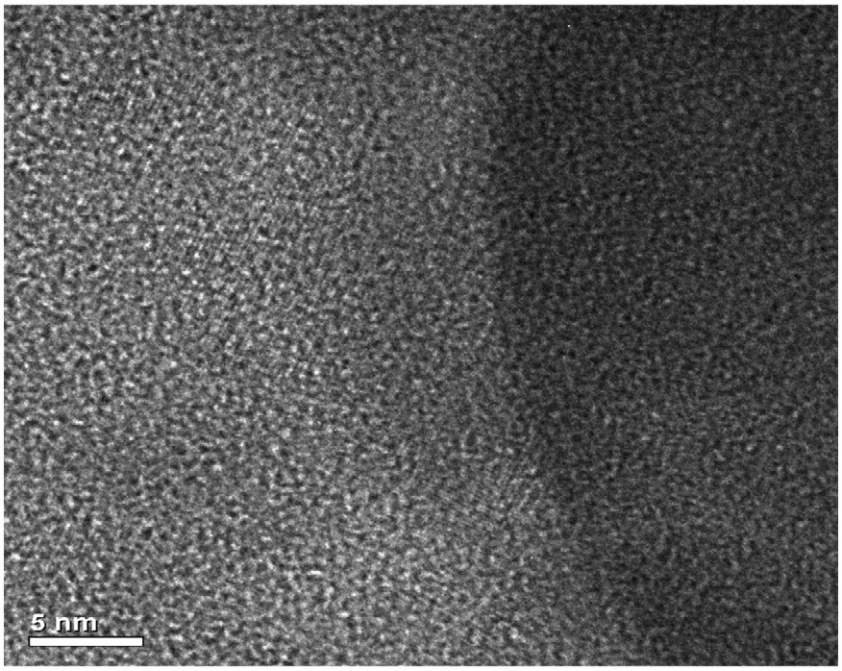

Fig. 3. HRTEM image of La_2NiO_4 coating after being heated in N_2 at 800 °C.

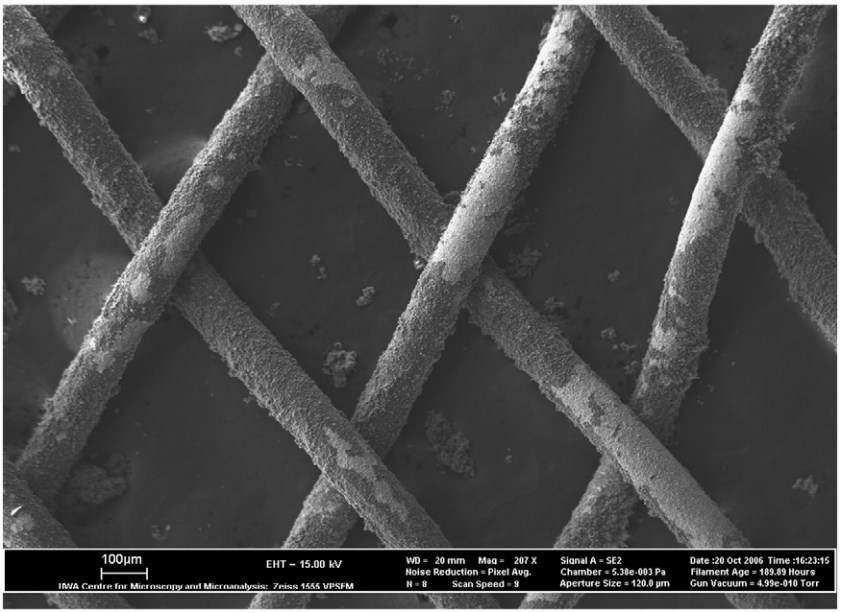

Fig. 4. The raw SS mesh (without sand blasting) loaded with La_2NiO_4.

the weakly attached catalyst on the mesh, the mesh was blown with compressed air and washed in the ultrasonic bath. Thus, only the firmly attached catalyst remained on the mesh.

2.2. Catalytic cracking of CH_4

The mesh coated with catalyst (ca. 0.3 g) was hold in the middle part of a quartz tube reactor (o.d. ~20 mm). The quartz tube was then positioned into a horizontal tubular furnace for catalytic reaction. Carbon fibers were grown by flowing CH_4/N_2 into the quartz tube. The detailed procedures were: (i) the mesh sample was heated in He (30 ml/min) at 800 °C for 1 h; (ii) the sample was reduced in a flow of H_2/N_2 (v/v, 10/90, 30 ml/min) at 800 °C for 1 h to obtain the nano-sized metal catalyst; (iii) the nitrogen diluted CH_4 was fed into the reactor at 800 °C for cracking over a 2 h period; and (iv) the mesh sample was cooled down in a He stream to room temperature. During methane decomposition, the effluent gases were analyzed by the gas chromatography (GC) (Shimazu GC-8A) on-line.

2.3. Characterization

Crystallographic information of carbon products was obtained by analyzing powder X-ray diffraction (XRD) (Shimadzu 6000) using filtered Cu Kα radiation as the X-ray source ($\lambda = 1.5406$ Å). High resolution transmission electron microscopes (HRTEM) (JEOL 3000F FEGTEM), transmission electron microscope (TEM) (JEOL, JEM 2010) and field emission scanning electron microscope (FESEM) (JEOL, JSM 7600F) were used to observe the morphologies of La_2NiO_4 catalyst on the SS mesh and carbon products. Laser Raman spectra were recorded using a Nicolet 560 FT Raman spectrometer with a He–Ne laser operating at a power of 1 mW. The BET specific surface area was measured using a Nova instrument.

3. Results and discussion

3.1. La_2NiO_4 coating on SS mesh

Fig. 1 shows the SEM image of SS after blasting with fine sand. The mesh surface was rough. The specific surface area of the raw SS mesh without any treatment was only 0.01 m^2/g while sand blasting increased it to 0.03 m^2/g. Even though the measurement of so small surface area was of big experimental error, it was obvious that the rough surface had higher surface area than the smooth one. Fig. 2a, b, and c show the morphologies of SS mesh coated with La_2NiO_4 after being

Table 1
The weights of SS mesh loaded with catalyst and carbon

CH_4 (in N_2)	Fresh SS mesh (g)	SS+ La_2NiO_4 (g)	SS+ reduced La_2NiO_4 (g)	C+SS+ reduced La_2NiO_4 (g)	Net C produced (g)	After compressed air blow (g)	After ultrasonication (g)	Net C remained (g)
5%	0.2968	0.3039	0.3002	0.3170	0.0168	0.3125	0.3086	0.0084
10%	0.2974	0.3044	0.3009	0.3250	0.0241	0.3200	0.3024	0.0015
30%	0.2942	0.3015	0.2989	0.5142	0.2153	0.4989	0.4359	0.1370
50%	0.2976	0.3048	0.3011	0.4494	0.1483	0.4057	0.3930	0.0919
70%	0.2965	0.3036	0.3000	0.3250	0.0250	0.3198	0.3097	0.0097
100%	0.2972	0.3047	0.3010	0.3200	0.0190	0.3179	0.3039	0.0029

heated at 800 °C in N_2. Calcination at 800 °C turned the precursor slurry into the La_2NiO_4 perovskite-like structure [21]. The mesh had been blown by compressed air and treated in an ultrasonic bath so that the weakly attached La_2NiO_4 particles were detached. The La_2NiO_4 catalyst covered the wire mesh surface evenly (see Fig. 2b). The La_2NiO_4 round particles were about 0.2 μm in size (see Fig. 2c). The HRTEM image of La_2NiO_4 is shown in Fig. 3 showing the fine lattice structure. There is speculation that there is an interaction between the mesh and La_2NiO_4 catalyst. It was found that most of the catalyst particles were detached from the mesh when blasted with compressed air and subjected to ultrasonic treatment if the mesh was not first sandblasted (see Fig. 4). Table 1 lists the weights of fresh mesh (sand blasted) and mesh loaded with La_2NiO_4, reduced-La_2NiO_4 (i.e. $Ni+La_2O_3$) and carbon generated by the methane cracking process (methane concentration: 5%–100%). Each of the six mesh samples (one batch) was loaded with approximately 2.4 wt.% of La_2NiO_4. The

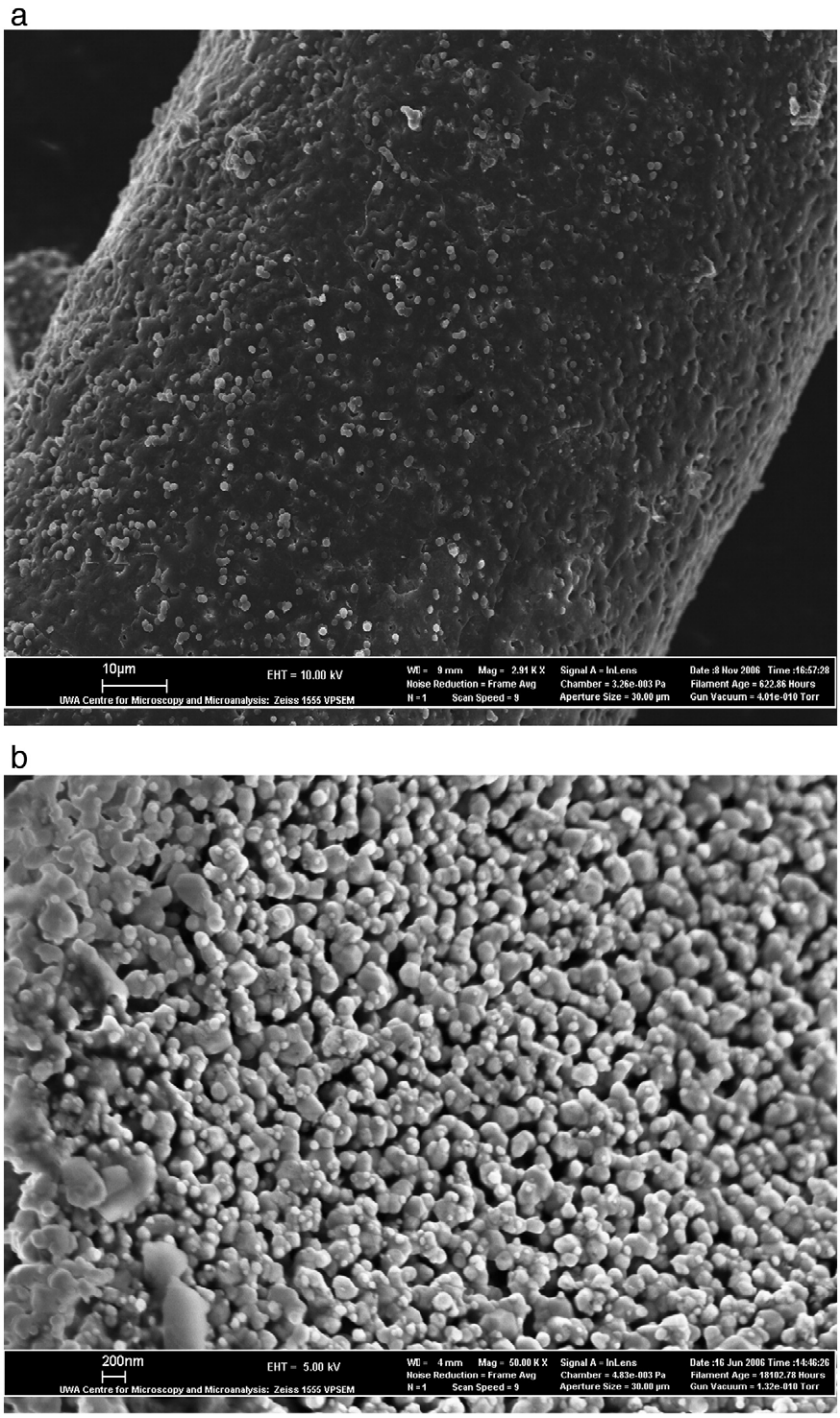

Fig. 5. SEM images (a and b) and HRTEM image (c) of the H_2-reduced La_2NiO_4 ($Ni–La_2O_3$) catalysts on the SS mesh.

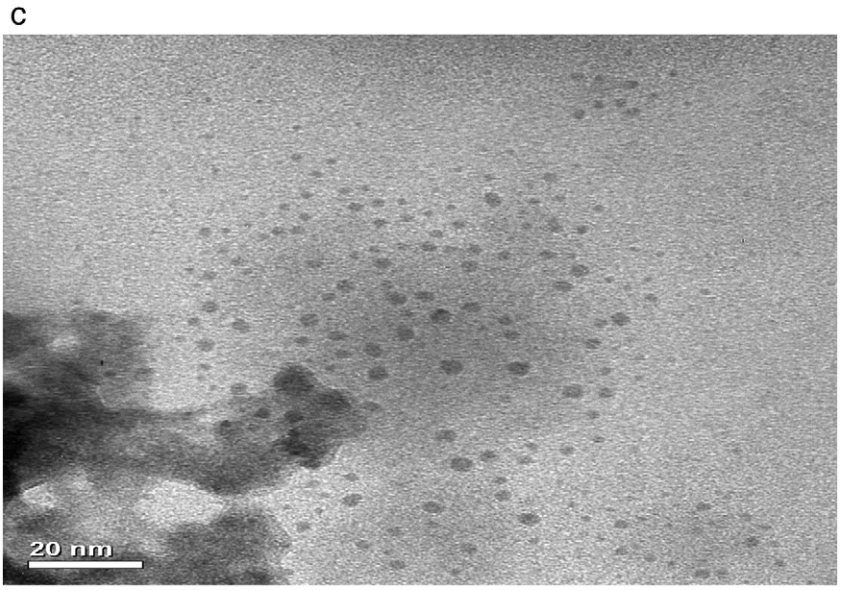

Fig. 5 (*continued*).

average specific surface area of La_2NiO_4/SS was approximately 1.2 m^2/g. Prior to methane cracking, the La_2NiO_4/SS was reduced in hydrogen to create Ni nano catalysts [20,21]. Because of the defined structure of perovskite-like La_2NiO_4, after reduction, the Ni nano metals were separated regularly with La_2O_3 to avoid agglomeration at high cracking temperatures. X-ray powder diffraction analysis could not be directly performed on the mesh and the amount of sample collected from the mesh was not enough to do the powder XRD study. In our previous study, the H_2 reduction of the powder La_2NiO_4 produced La_2O_3 and metallic nickel; We tentatively assumed that the reduction behavior of La_2NiO_4 film on the mesh was similar to the La_2NiO_4 powder [20,33].

Fig. 5a and b show the SEM images of the H_2-reduced La_2NiO_4 (or Ni–La_2O_3) catalyst on the SS mesh. The catalyst particles became smaller and more isolated in comparison with the non-reduced catalyst shown in Fig. 2c — they were nano sized and were evenly dispersed on the mesh surface. Even

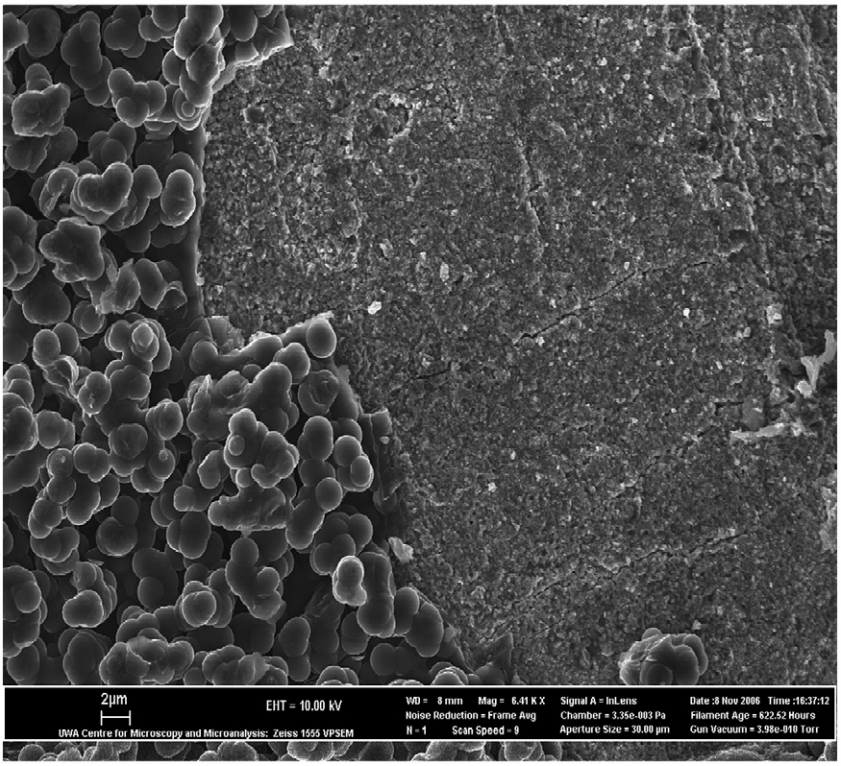

Fig. 6. SEM image of the mesh partially covered with catalyst.

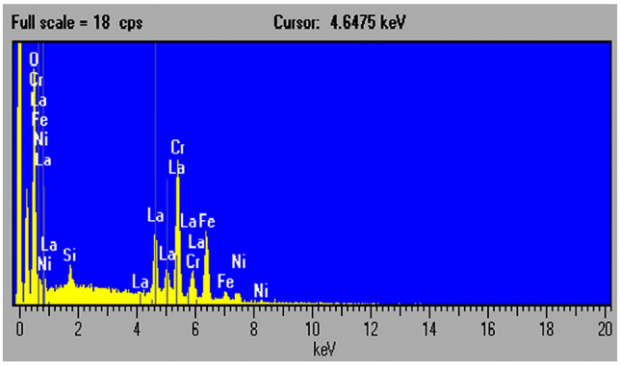

Fig. 7. EDX spectrum of (Ni+La_2O_3)SS.

though the mesh was put into the ultrasonic bath for 1 h, the catalyst remained strongly attached to the SS mesh. A sample of H_2-reduced catalyst was scratched from the mesh and observed under the HRTEM; the image is shown in Fig. 5c. The black particles were identified as nickel metals of approximately 5 nm in diameter.

After reduction, approximately 1.1 wt.% nano catalyst (Ni+La_2O_3) remained on the mesh. It was impossible that the observed weight loss was only caused by the reduction of La_2NiO_4 to La_2O_3 alone. It is speculated that Fe_2O_3, NiO, Cr_2O_3 and Mn_2O_3 over the stainless steel surface were also reduced at the same time. The average specific surface area was enhanced from 1.2 m^2/g to 1.8 m^2/g. The reduction of La_2NiO_4 produced La_2O_3 and Ni^o metals. Normally, the metal particles were easily sintered at high temperatures. In the application of the nano catalyst it is difficult to immobilize the nano metals and one effective solution is to deposit the catalyst precursors on zeolites or other porous materials to template and immobilize the nano structures. However, most of the zeolites are unstable at temperatures above 800 °C. In the reduced La_2NiO_4 structure, Ni was separated by La_2O_3 and it was speculated that there was a strong interaction between the SS mesh and the nano catalyst (Ni+La_2O_3). Fig. 6 shows the SEM image of the mesh partially covered with catalyst; note that some catalyst was removed earlier for HRTEM analysis. During SEM observation, we estimated that catalyst was around 50 nm in thickness. The elements contained in the (Ni+La_2O_3)/SS sample were analyzed by using the energy dispersive X-ray (EDX) technique. The EDX spectrum shown in Fig. 7 indicated that there were elements of Fe, La, Ni, Cr and Si. The Fe, Ni, Cr and Si were the elements in SS. La and Ni were the components of the catalysts. This result indicated that actually the La_2NiO_4 film had been loaded on the SS mesh.

3.2. Methane cracking

Fig. 8 shows a plot of the methane conversion *vs* the reaction temperature over the H_2-reduced La_2NiO_4/(Ni+La_2O_3)/SS mesh catalyst. By varing the methane concentration from 5% to 100%, the methane conversion always reached its maxmium at the temperature of 750 °C. The methane conversion decreased with the rise of concentration. The highest methane conversion was 32.5% when the feed gas included 5% methane at 750 °C. Diluted methane had a lower space velocity over the fixed weight mesh catalyst and generally the lower space velocity resulted in higher conversion. Table 1 indicated that the 30% methane produced the maximum amount of carbon attached to the SS mesh and it was observed that the compressed air blow and ultrasonic treatment caused some carbon products to detach from mesh. The mesh was weighted until the weight reached a constant value and the results were recorded in Table 1. Using an approximately 0.3 g SS mesh, 5%, 10%, 30%, 50%, 70% and 100% methane cracking produced 0.0168 g, 0.0241 g, 0.2153 g, 0.1483 g, 0.0250 g and 0.0190 g carbon products, respectively; after repeated compressed air-blow and ultrasonic treatment, there were still 0.0084 g, 0.0015 g, 0.1370 g, 0.0919 g, 0.0097 g and 0.0029 g of carbon products remaining on the mesh respectively. At a temperature of 750 °C and CH_4 pressure at 101 kPa, over the catalysts of Ni/SiO_2, Cu–Ni/SiO_2, Rh–Ni/SiO_2, Pd–Ni/SiO_2, Ir–Ni/SiO_2, Pt–Ni/SiO_2, Pd/SiO_2, Pd–Ni/Al_2O_3, Pd–Ni/TiO_2, Pd–Ni/MgO and Pd–Ni/CF (carbon fiber), it was found that the methane conversions were all below 15% [34]. At 500 °C and CH_4 pressure of 101 kPa and catalysts of Co/SiO_2, Co/TiO_2, Co/MgO and Co/Al_2O_3, the methane conversions were all below 10% [35]. Using the Ni–Cu/Al_2O_3 catalyst, at 500 °C, 600 °C, 700 °C and 750 °C, the methane (undiluted) conversions were around 10%, 22%, 59%, and 65% respectively [36]. Alternatively, using a Ni–SiO_2 catalyst, methane (20% in N_2) conversion was ca. 36% at 750 °C after 50 min [37]. Despite the lower loading of the La_2NiO_4 catalyst on the SS mesh, the catalytic activity of La_2NiO_4/SS mesh was competitive to traditional powder catalysts. We roughly investigated the influence of pressure on the methane conversion and the morphology of the carbon product. The higher pressure resulted in the lower conversion efficiency of methane, but there was no significant change in the morphology of the carbon product.

3.3. Characterization of the carbon products

Fig. 9a shows the SEM image of the carbon coated mesh (C/La_2NiO_4/SS) (30% methane cracking). Fig. 9b, c, d, e, f, and g

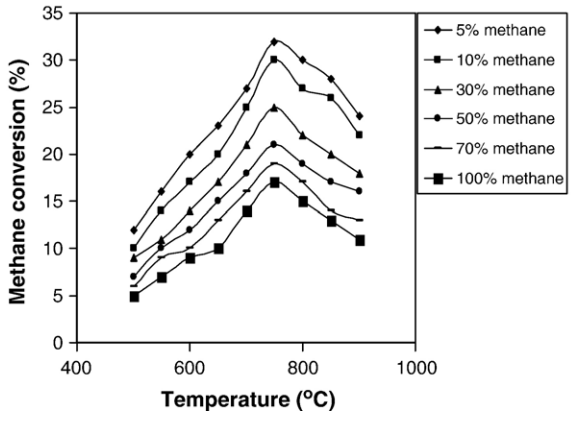

Fig. 8. The temperature-dependence of methane conversion over the H_2-reduced La_2NiO_4/SS catalyst.

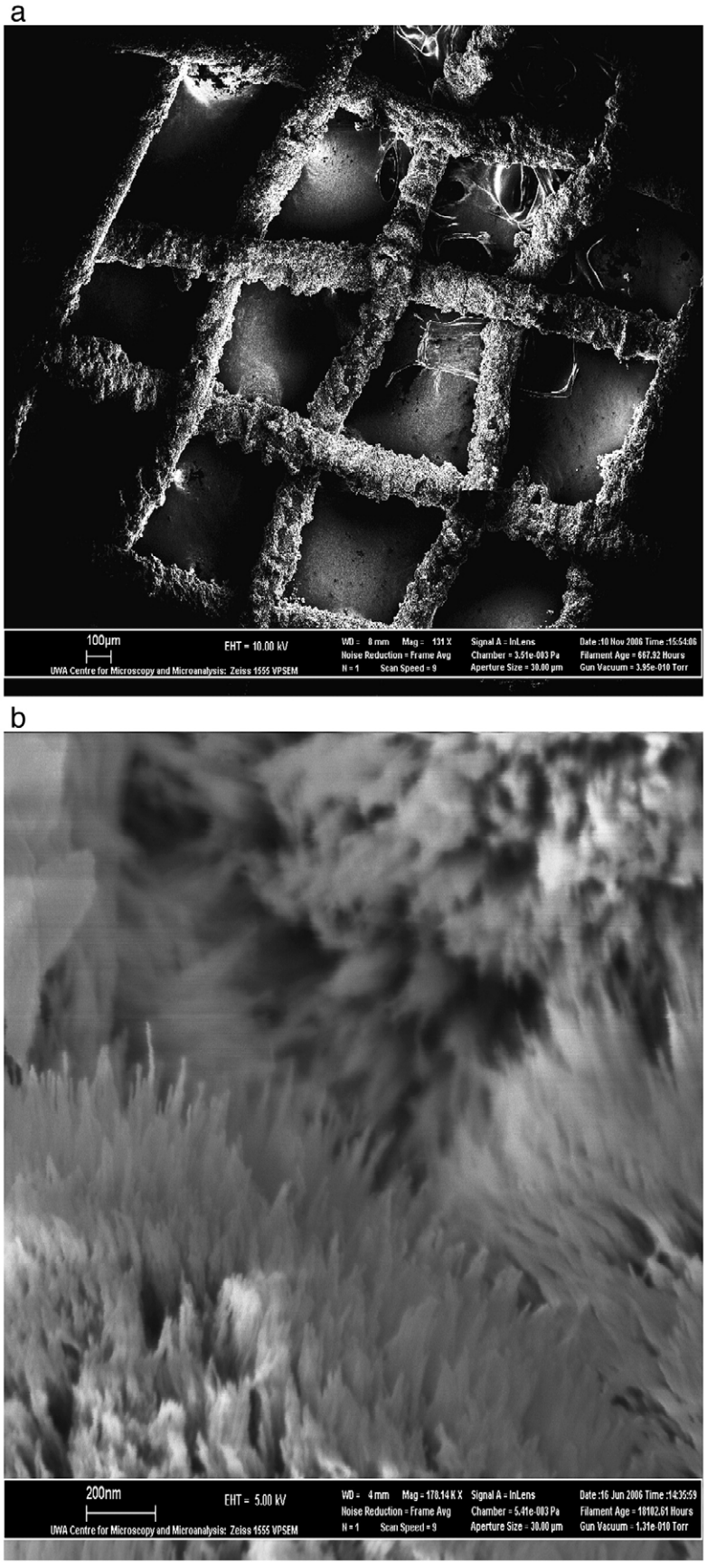

Fig. 9. (a) SEM image of the carbon coated mesh ($C/La_2NiO_4/SS$) (30% methane cracking). SEM images of carbon products obtained by the cracking of methane in a concentration of (b) 5%, (c) 10%, (d) 30%, (e) 50%, (f) 70% and (g) 100% methane.

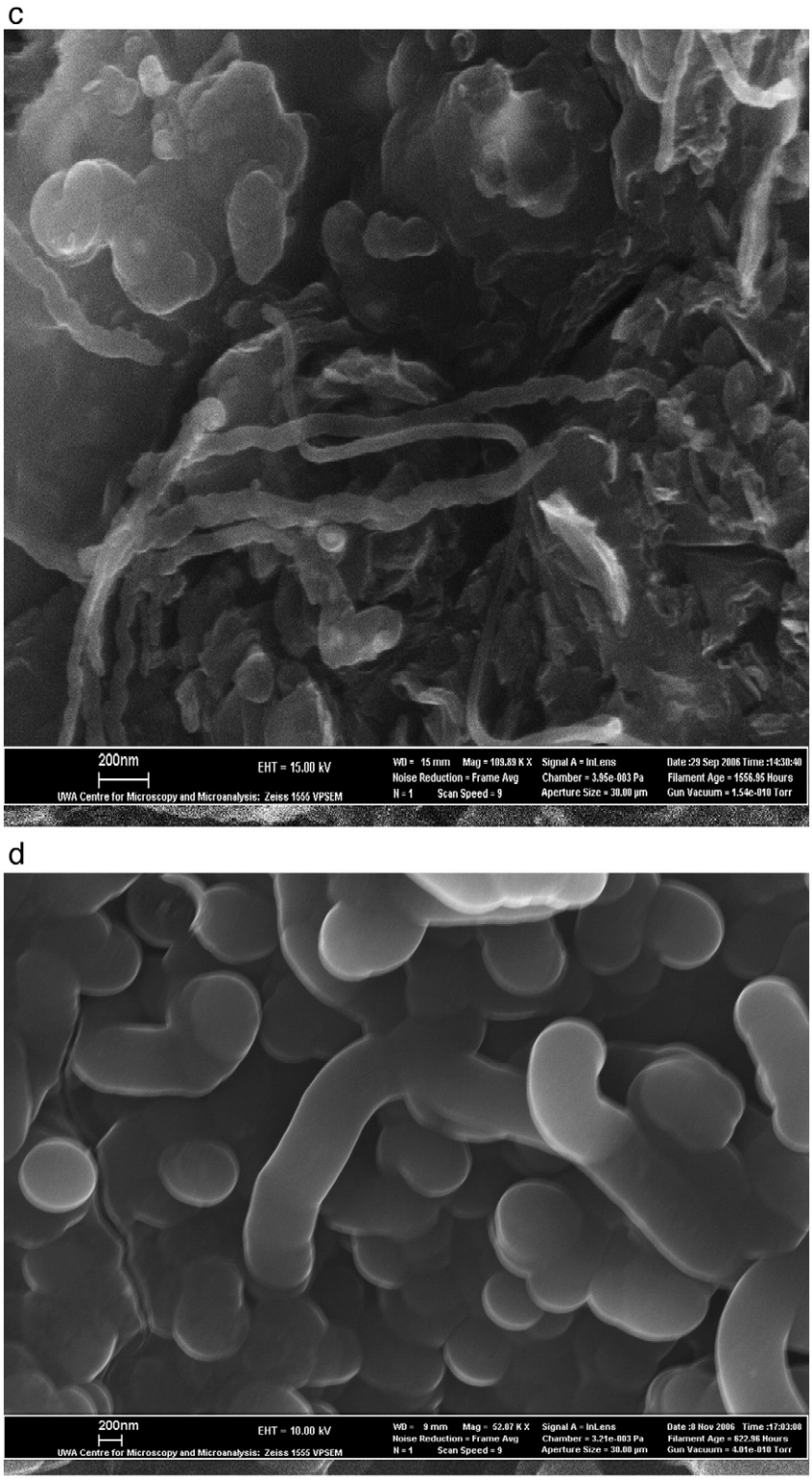

Fig. 9 (*continued*).

show the carbon attached to the mesh generated by cracking methane in the concentrations of 5%, 10%, 30%, 50%, 70% and 100%, respectively. In general, the carbon products were fibers together with round particles. 5% methane cracking generated carbon fibers with diameter at around 20 nm (see Fig. 9b). Fig. 9b shows that the as-grown nanotubes are in vertically aligned form; The growth of carbon nanotubes probably adopted the bass-model with catalyst particles sited at the bottom of each nanotube, given the strong adhesion of the catalyst layer to the mesh substrate. Samples of carbon were scraped from the mesh and observed under TEM and found it consisted of nanofibers with hollow tubes with a mean inner

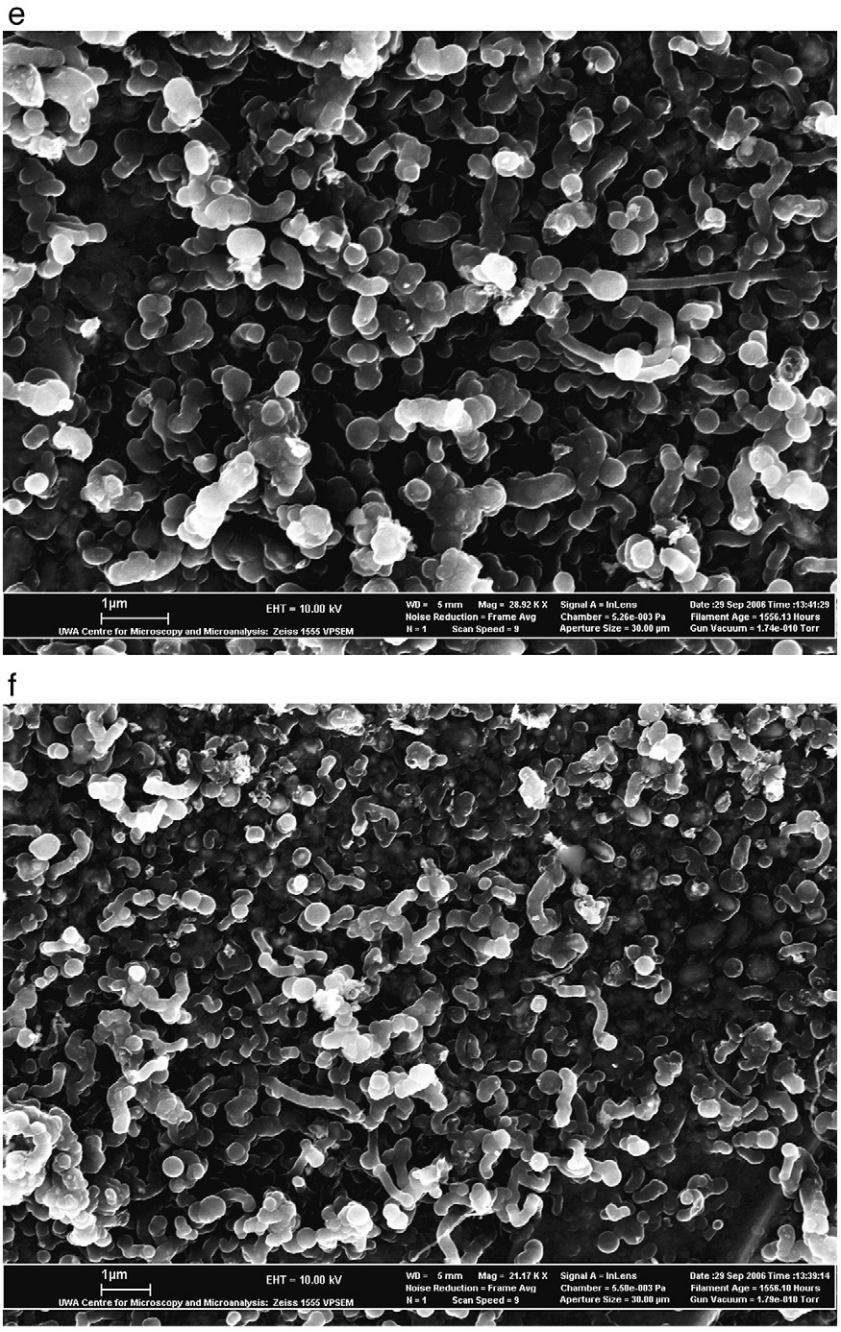

Fig. 9 (*continued*).

diameter of 20 nm. The HRTEM indicated that the tubes were composed of ca. 30 layers (Fig. 10). By increasing the methane concentration, the fiber became thicker. 10%, 30%, 50%, 70% and 100% methane produced the carbon fibers with a diameter at ca. 100 nm, 300 nm, 300 nm, and 400 nm respectively; However, 10–100% methane cracking did not generate carbon nano tubes. The exact mechanisms for the growth of hollow nanotubes and solid fibers were not clear. It is assumed that when the methane concentration was 5%, the carbon growing rate was slow, allowing the fibers to build up a hollow structure. Alternatively, when the methane concentration was high, the carbon accumulation was fast, producing a solid fiber instead of a hollow tube. Fig. 11 shows the HRTEM of the carbon solid fibers obtained from 30% methane cracking, allowing the fringes of graphite sheets to be clearly observed. The carbon is of graphitic structure, with no hollow tube structures detected. There were many defects in the graphitic sheets observed. The graphene layer appeared to be herringbone structure. Fig. 12a and b show the EDX spectra of the mesh and catalyst with carbon generated by 5% and 30% methane cracking respectively. Fig. 12a also shows that there are peaks of Ni and C. Because of the carbon coverage, the other elements in the SS mesh were not detected. Strong Ni peaks appeared, but without associated La peaks; This observation suggested that Nano Ni

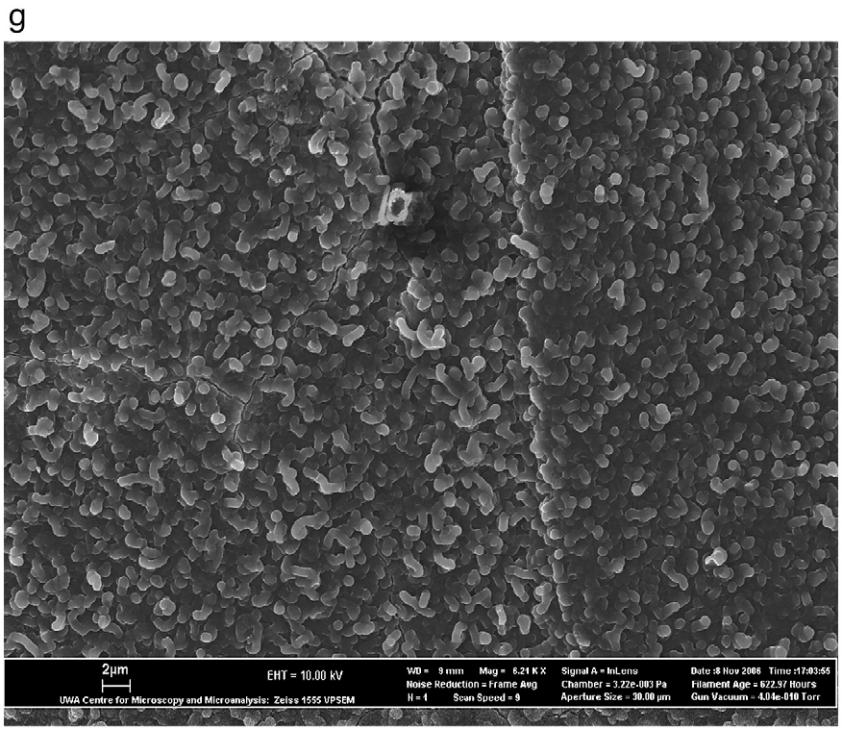

Fig. 9 (*continued*).

metals were the cracking catalysts. Fig. 12b shows that only carbon peaks were detected. One reason was that the carbon fiber layer was too thick and the nickel concentration was too low to be detected. The other possible reason was that the nickel nano metals were attached to the root of carbon solid fibers.

Phase identification of the carbon products was carried out using the XRD technique. The process involved cutting the coating from the mesh and analyzing it with the XRD. Fig. 13 shows the XRD patterns of the carbon obtained by 5% and 30% methane cracking. The diffraction peak at $2\theta = 26.32$ was graphite (002) reflections of hexagonal graphite (JCPDS Card Files, No. 41-1487) [38], indicating that the carbon fibers were highly graphitic. The peaks at 43.8/44.4, 50.96/51.6 and 76.4/77.0 were the diffraction of metallic Ni° [22,37]. This observation demonstrated that the metallic nickel was the active site for the growth of carbon tubes/fibers. The carbon product coexisted with the nickel catalyst.

Fig. 14a and b show the Raman spectra of the carbon fibers obtained by cracking 5% and 30% methane at 800 °C for 2 h

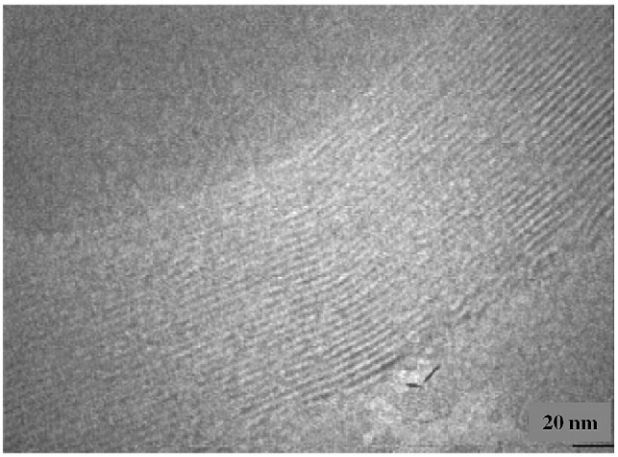

Fig. 10. HRTEM images of the carbon obtained by cracking 5% methane.

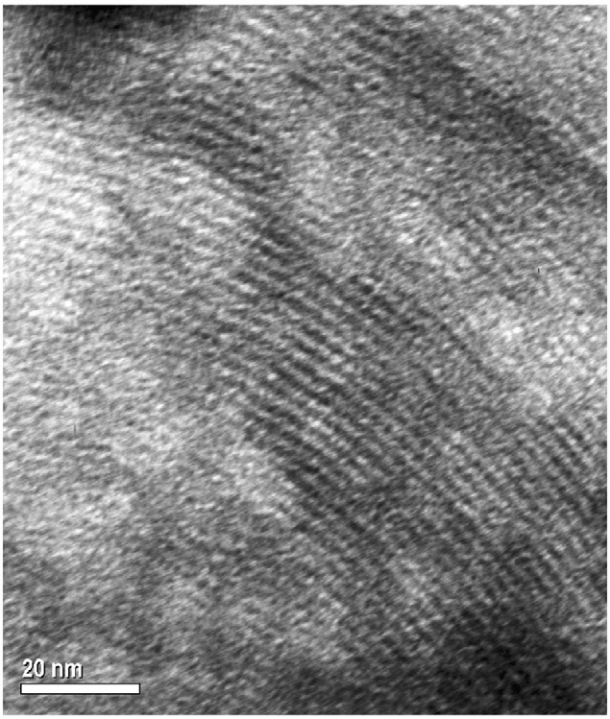

Fig. 11. HRTEM of the carbon solid fibers obtained from 30% methane cracking.

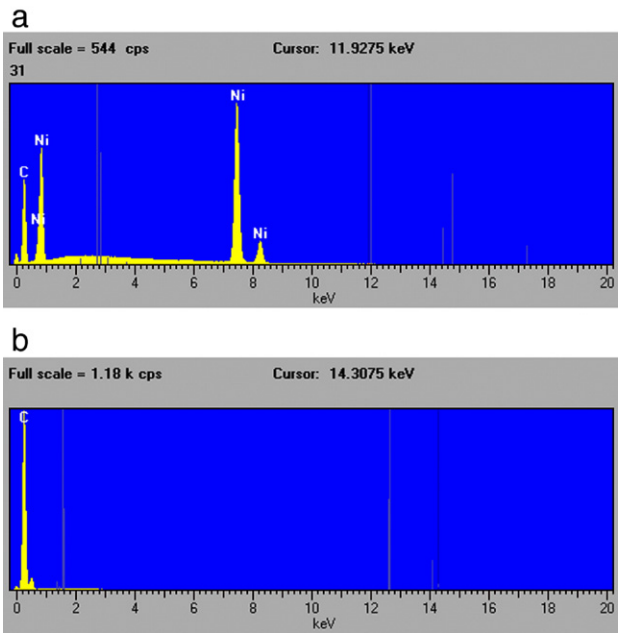

Fig. 12. EDX spectra of the SS mesh coated with catalyst and carbon products generated by cracking of (a) 5% and (b) 30% methane.

respectively. These were detected in bands at 1568 cm^{-1} (G band) and 1341 cm^{-1} (D band). It was known that the D band was usually associated with the vibrations of carbon atoms with dangling bands for the in-plane terminations of carbon atoms of disordered graphite, while the G band was closely related to the vibration in all sp^2 bonded carbon atoms in a two-dimensional hexagonal lattice, such as in a graphite layer. I_D/I_G could be used as an indicator of the extent of disorder within the graphitic

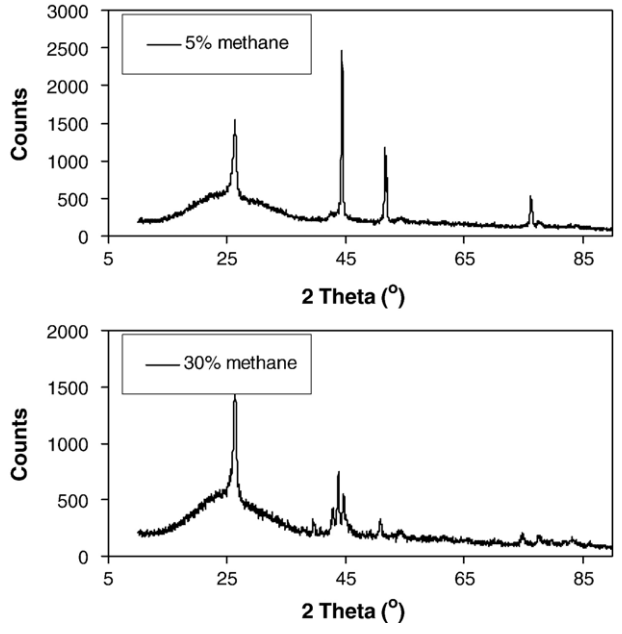

Fig. 13. XRD patterns of the carbon products obtained by cracking 5% and 30% methane.

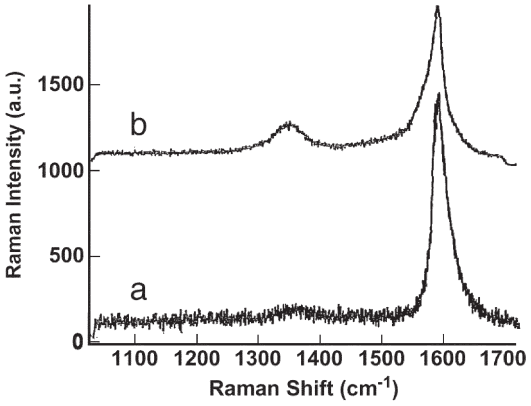

Fig. 14. Raman spectra of the carbon products obtained by cracking (a) 5% and (b) 30% methane.

layer [39]. The D band in the spectrum of Fig. 14a was weaker than that of Fig. 14b while the G band in the spectrum of Fig. 14a was stronger than that in Fig. 14b. These results indicated that there were more defects in the carbon microfibers obtained by cracking at 30% methane than that in the carbon nanotubes obtained by cracking at 5% methane.

3.4. BET specific surface area

Table 2 lists the BET specific surface area of the SS mesh after carbon coating and respective post treatment. The BET specific surface area of fresh SS mesh was only 0.01 m^2/g, but after catalyst loading (H_2-reduced La_2NiO_4/SS), it increased to 1.80 m^2/g. The carbon coating enhanced the specific surface area significantly. The 5%, 10%, 30%, 50%, 70% and 100% methane cracking increased the specific area to 51.8 m^2/g, 42.3 m^2/g, 39.4 m^2/g, 32.7 m^2/g, 30.18 m^2/g and 28.3 m^2/g respectively after the compressed air blow. The following sonication made it drop to 45.2 m^2/g, 38.5 m^2/g, 33.0 m^2/g, 28.4 m^2/g, 24.6 m^2/g and 21.7 m^2/g respectively. The cracking of lower concentration methane gave a higher surface area enhancement; suggesting the increased area was the result of the thinner fibers, particularly the nanotubes with larger specific surface area. This work indicates that C/SS material has a great application potential for use with catalyst. The aluminum coated SS mesh by electrophoretic deposition was only 12.23 m^2/g [7].

Table 2
The BET specific surface area of the SS mesh loaded with catalyst and carbon

CH_4 concentration In N_2	Surface area after compressed air blow (m^2/g)	Surface area after ultrasonication (m^2/g)
5%	51.8	45.2
10%	42.3	38.5
30%	39.4	33.0
50%	32.7	28.4
70%	30.1	24.6
100%	28.3	21.7

4. Conclusion

i) La_2NiO_4 catalyst was loaded firmly on the stainless steel mesh support and H_2-reduction was carried out to generate regular nano metal catalysts on the mesh surface.
ii) The methane cracking process deposited dense carbon fibers together with globular carbon particles onto the mesh. The 5% methane produced multiwalled carbon nanotubes (i.d. ~20 nm, 30 walls). 10%–100% methane cracking generated carbon solid fibers (ca. 100 nm–400 nm). The carbon tubes or fibers were firmly attached to the mesh and could withstand the compressed air blow and ultrasonic treatment.
iii) The carbon products were of graphitic structure and it was found that there were more defects in the fibers than in the tubes.
iv) The carbon tubes/fibers coating on the SS mesh improved the specific surface area of SS mesh from 0.01 m^2/g to several decades of m^2/g.

Acknowledgments

We thank Rob Greenhalgh for the English language correction of the text.

References

[1] M.V. Twing, D.E. Webster, A. Cybulski, J.A. Moulijn, Structured Catalysis and Reactors, Marcel Dekker, New York, 1998.
[2] G. Ertl, H. Knözinger, J. Weitkamp, Environmental Catalysis, Wiley-VCH, Weinheim, 1999.
[3] C.N. Satterfield, Heterogeneous Catalysis in Industrial Practice, (second ed.)McGraw-Hill, New York, 1991.
[4] J.R. Gibbins, Investigation of primary coal pyrolysis processes using a variable heating rate wire mesh apparatus. Ph.D Thesis, University of London, London, U.K. (1988).
[5] A.R.F. Drummond, I.W. Drummond, Ind. Eng. Chem. Res. 35 (1996) 1263.
[6] R.C. Messenbock, D.R. Dugwell, R. Kandiyoti, Fuel 78 (1999) 781.
[7] K.S. Yang, Z. Jiang, J.S. Chung, Surf. Coat. Technol. 168 (2003) 103.
[8] K.H. An, W.S. Kim, Y.S. Park, J-M. Moon, D.J. Bae, S.C. Lim, Y.S. Lee, Y.H. Lee, Adv. Funct. Mater. 11 (2001) 387.
[9] C. Srividya, I. Moskowitz, S.V. Babu, J. Mater. Res. 14 (1999) 2124.
[10] F. Airoldi, A. Colombo, D. Tavano, G. Stankovic, S. Klugmann, V. Paolillo, E. Bonizzoni, C. Briguori, M. Carlino, M. Montorfano, F. Liistro, A. Castelli, A. Ferrari, F. Sgura, C. Di Mario, Am. J. Cardiol. 93 (2004) 474.
[11] L. Valentini, A. Di Schino, J.M. Kenny, Tribol. Lett. 16 (2004) 51.
[12] M. Karwa, Z. Iqbal, S. Mitra, J. Mater. Chem. 16 (2006) 2890.
[13] W. Qian, T. Liu, F. Wei, Z. Wang, Y. Li, Appl. Catal. A 258 (2004) 121.
[14] N.R. Franklin, Y. Li, R.J. Chen, A. Javey, H. Dai, Appl. Phys. Lett. 79 (2001) 4571.
[15] Y. Murakami, Y. Miyauchi, S. Chiashi, S. Maruyama, Chem. Phys. Lett. 377 (2003) 49.
[16] L. Delzeit, B. Chen, A. Cassell, R. Stevens, C. Nguyen, M. Meyyappan, Chem. Phys. Lett. 348 (2001) 368.
[17] D. Méhn, A. Fonseca, G. Bister, J.B. Nagy, Chem. Phys. Lett. 393 (2004) 378.
[18] Y. Chen, D. Ciuparu, S. Lim, Y. Yang, G.L. Haller, L. Pfefferle, J. Catal. 225 (2004) 453.
[19] B.C. Liu, L.Z. Gao, Q. Liang, S.H. Tang, M.Z. Qu, Z.L. Yu, Catal. Letters 71 (2001) 225.
[20] Q. Liang, L.Z. Gao, Q. Li, S.H. Tang, B.C. Liu, Z.L. Yu, Carbon 39 (2001) 897.
[21] H. Li, Q. Li, L.Z. Gao, C.T. Au, Z.L. Yu, Catal. Lett. 74 (2001) 185.
[22] L.P. Zhou, K. Ohta, K. Kuroda, L. Ni, L.Z. Gao, T. Matsumoto, J. Nakamura, J. Phys. Chem. B 109 (2005) 4439.
[23] P.H. Cuong, R. Vieira, B. Louis, A. Carvalho, J. Amadou, T. Dintzer, J. Catal. 240 (2006) 194.
[24] L. Randall, W. Vander, J.H. Lee, Carbon 41 (2003) 659.
[25] M.F. de Riccardis, D. Carbone, Th. Dikonimos Makris, R. Giorgi, N. Lisi, E. Salernitano, Carbon 44 (2006) 671.
[26] S.S. Tzeng, K.H. Hung, T.H. Ko, Carbon 44 (2006) 859.
[27] J.W. Geus, J.C. van Giezen, Catal. Today 47 (1999) 169.
[28] A.F. Ahlström-Silversand, C.U. Ingemar Odenbrand, Appl. Catal. A 153 (1997) 177.
[29] L. Pranevicius, L.L. Pranevicius, P. Valatkevicius, V. Valincius, Surf. Coat. Technol. 123 (2000) 122.
[30] X. Nie, A. Leyland, H.W. Song, A.L. Yerokhin, S.J. Dowey, A. Matthews, Surf. Coat. Technol. 116-119 (1999) 1055.
[31] P. Sarkar, P.S. Nicholson, J. Am. Ceram. Soc. 79 (1996) 1987.
[32] M.P. Vorob'eva, A.A. Greish, A.V. Ivanov, L.M. Kustov, Appl. Catal. A 199 (2000) 257.
[33] J.Z. Luo, L.Z. Gao, C.F. Ng, C.T. Au, Catal. Lett. 62 (1999) 153.
[34] S. Takenaka, Y. Shigeta, E. Tanabe, K. Otsuka, J. Catal. 220 (2003) 468.
[35] S. Takenaka, M. Ishida, M. Serizawa, E. Tanabe, K. Otsuka, J. Phys. Chem. 108 (2004) 11464.
[36] J. Chen, Y. Li, Z. Li, X. Zhang, Appl. Catal. A 269 (2004) 179.
[37] T. Zhang, M.D. Amiridis, Appl. Catal. A 167 (1998) 161.
[38] G. Xi, M. Zhang, D. Ma, Y. Zhu, H. Zhang, Y. Qian, Carbon 44 (2006) 734.
[39] Y.T. Lee, J. Park, Y.S. Choi, H. Ryu, H.J. Lee, J. Phys. Chem. B, 106 (2002) 7614.